Technology Requirements in Advanced Microwave Radiometry

A Technology Definition Study For NASA ESTO

Contributors

Langley Research Center
J.W. Johnson
R.W. Lawrence
M.C. Bailey

University of Massachusetts
C.T. Swift
D.M. Pozar
S..D. Targonski

Goddard Space Flight Center
D.M. LeVine

December 15, 1998

Contents

Executive Summary

The state-of-the-art in spatial resolution for passive microwave remote sensing from space has progressed very little since its beginnings with ESMR. Even the successful Special Sensor Microwave/Imager (SSM/I) employs an antenna dish of less than 1 meter and does not include channels at the lowest end of the microwave spectrum. Needs in the future include high performance (□Tand stability) at lower frequencies and an order of magnitude improvement in spatial resolution. The object of this study is to define the technology development needed to meet these future requirements.

The approach adopted to identify the technology needed in the future was to consider the requirements of two reference missions that today embody major measurement challenges. These are the measurement of salinity and temperature in the open ocean, which requires sensitivity and stability on the order of .05 K, and the measurement of soil moisture and salinity in the coastal zone, which requires very high spatial resolution, with antennas 15-20 m in diameter. Trade studies were performed to determine which sensor technology paths offered the best promise for meeting the goals of these two missions and what critical components needed to be developed to enable these sensors.

To meet the needs for extreme radiometric sensitivity and precision, the study suggested that scanning real aperture systems (such as SSM/I) had the most promise. However, technology development in Receiver Technology and in Deployable Arrays and Materials is needed to realize the potential of these systems. MMIC integrated front-ends, high precision/high stability receiver architectures, and low power/highly stable noise sources are required to reach .05 K precision and stability. In addition, concepts for low-loss, lightweight antennas and materials technology for reflectors are required.

To meet future needs in high spatial resolution, the study identified two new sensor technologies, which are two-dimensional synthetic aperture radiometers and pushbroom radiometers. To enable aperture synthesis in two dimensions, technology development is needed in Array Optimization and Imaging, Instrument Architectures, and Signal Processing and Correlation. Needs include arrays that provide optimal surface sampling and image correction techniques for optimal pixel averaging. Validation with 2D aircraft radiometers is needed to determine how to maximize swath and □T in high spatial resolution measurements. Techniques for minimizing errors due to signal distribution over large arrays, for example by RF direct sampling, and techniques for providing phase calibration over distributed systems for coherence are also required. The large number of channels in 2D synthetic aperture systems requires low power devices and techniques for digital I/Q detection and digital correlation. Pushbroom systems require technology

development in receivers and deployable arrays similar to real aperture systems, and in phase calibration techniques similar to synthetic aperture systems.

1.0 Introduction

The Special Sensor Microwave/Imager (SSM/I) represents the current capability in spaceborne microwave radiometry for earth sciences. After its launch, it soon became evident that the quality of the data was considerably superior to that provided by its predecessors (the ESMR and SSMR on NIMBUS and SeaSat, respectively). This level of performance was achieved through instrument stability and calibration techniques, and led to high quality geophysical retrievals including sea ice age and extent, atmospheric cloud liquid and water vapor, and ocean surface wind speed. In addition, its stability enabled the retrieval of weaker effects such as ocean surface wind direction. Given the SSM/I experience, the passive microwaves challenge for earth sciences now is to realize similar success over a wider range of operating frequencies and with greater performance to meet a larger set of science needs. The objective of this study was to define the technology development required to meet this challenge.

The purpose of this report is to document the study and its results. The rationale determining the scope of the study will be explained, a set of parametric analyses used in defining system concepts and requirements will be described, and detailed technology solutions requiring development in order to enable particular science measurement capabilities will be recommended. A tutorial level of rigor, concentrating on principles and issues, was followed in the trade studies and analysis work in order to provide as broad a treatment of alternative measurement techniques and instrument concepts as possible. In some cases the technical points made won't be anything new to people in this field, but will provide context and background for the conclusions and recommendations to come.

Table 1 is a list of earth science measurements and corresponding microwave radiometric performance characteristics [1]. It was used in determining a realistic scope for this study and to help in establishing a structure for the study. One can see that the greatest demands in radiometric sensitivity and spatial resolution cluster around .05 K and 10 km, respectively. It was decided to limit the study to applications at the lower frequencies at L, S, and C Band, and to structure the study around meeting these strict performance requirements. Therefore, the study took a dual approach using two reference missions. The measurement of open ocean salinity and sea surface temperature with the ΔT and stability requirements of .05 K was used as one reference mission, and the measurement of soil moisture and coastal salinity with the spatial resolution requirement of 10 km was used as the other reference mission. Although there will be seen to be some overlap in technologies, these reference missions pretty clearly call for different instrument concepts. This study is not meant to select or promote a particular

mission or instrument concept but to discuss the conventional wisdom, to demonstrate pros and cons suggesting relative merits, and to identify particular difficulties.

Table 1. Measurements and Requirements Assumptions

Measurement	ΔT, K	Spatial Resolution, km	Frequency, GHz
Atmospheric Sounding	.05	50	22, 60, 118, 183
Ocean Salinity			1.4, 2.5, 6.8
Open Ocean	.05	100	
Coastal	0.5	< 10	
Sea Surface Temperature	0.2	10	2.5, 6.8
Soil Moisture	2.0	10	1.4, 2.5, 6.8
Ocean Winds	0.3	25	10, 18, 37
Sea Ice	1.0	< 10	1.4, 18, 37
Precipitation	1.0	10	6, 10, 95, 118
Snow Cover	1.0	10	1.4, 18, 37

The two reference missions, or the .05 K ΔT and stability requirement and the 10 km spatial resolution requirement, will be discussed separately, for the most part, in this report. Instrument concepts, trade-offs, and analyses will be treated separately for the two, but in the end an integrated technology development roadmap will be provided.

The section on .05 K performance at L-Band will use a mechanically scanned real aperture measurement concept as a basis. Device level performance requirements will be derived for a variety of front-end configurations and calibration techniques focusing on a cold sky and noise diode hot source calibration. This instrument concept is valid for meeting the high stability requirement where relatively low spatial resolution and something less than 10 m aperture size is needed. This concept is also readily adaptable to S and C band.

The conventional wisdom concerning candidate technologies for enabling the 10 km spatial resolution performance at L-Band will be reviewed. The rationale for stationary vs. mechanically scanning systems, advantages of the pushbroom approach and the potential for inflatable and membrane technology, and imaging by aperture synthesis in both one and two dimensions will be discussed. The two dimensional synthetic aperture concept is considered valid for meeting the high spatial resolution requirement at L-Band and will be used as a basis in identifying technology development needs. Selected pushbroom concepts requiring inflatable reflector technology and membrane array technology will also be described.

A technology development roadmap featuring the traditional mechanically scanning real aperture concept for the relatively small aperture high stability measurement, and synthetic aperture and pushbroom concepts for the very high spatial resolution measurement will be provided as a conclusion.

2.0 Design Alternatives for .05 K Precision and Stability

When viewing the earth, a microwave radiometer measures the brightness temperature, T_B, which is related to the absolute thermometric temperature T, through a constant of proportionality known as the emissivity e. Any information relating to the physical properties of the ocean, including salinity and surface roughness is contained within the emissivity, which is a complex function of the dielectric constant of sea water, viewing angle, polarization, and other factors. The dielectric constant, in turn, is governed by the ratio of the conductivity of sea water to the electromagnetic frequency. Since the conductivity is a well known, and strong function of salinity, the remote sensing measurement is enhanced by observing the ocean at low frequencies. The L-Band frequency of 1.4 GHz is a particularly attractive choice for a number of reasons, including acceptable measurement sensitivity. The average sensitivity is approximately 1 K change in brightness temperature for a 2 ppt change in salinity concentration. Since the useful measurement accuracy is 0.1 - 0.2 ppt over the open ocean, the accuracy and precision of the radiometer must be 0.05 - 0.1 K. Instrument precision is defined by the following equation:

$$\Delta T_B = \frac{T_{sys}}{\sqrt{B\tau}} \qquad (1)$$

Here, T_{sys} is the system noise temperature, and ΔT_B is the statistical fluctuation associated with a noisy measurement. The noise is reduced by the square root of the product of the instrument bandwidth B and the post detection integration time τ. In fact, the time bandwidth product is the number of independent samples that are averaged by the circuitry of the instrument. Since the bandwidth will nominally be fixed by the protected 27 MHz

radio astronomy band, our requirements on ultra high precision require us to minimize system noise temperature and maximize integration time. The system noise is comprised of the sum of the noise temperature introduced by the hardware and the scene being observed. At nadir, the scene temperature is about 100 K, thus, even if noise free RF amplifiers could be constructed, the scene itself defines a lower bound for T_{sys}. If the radiometer scans the earth from orbit the velocity of the spacecraft imposes a constraint on the integration time if the radiometer operates in an imaging mode. In fact, it has been shown [2], that an uncertainty relationship can be developed for imaging systems, such that;

$$\Delta T_B \Delta x = T_{sys} \sqrt{\frac{4\Delta vh}{B}} \tag{2}$$

where Δx is the pixel resolution of the image, "v" is the satellite velocity, and "h" is the satellite altitude. Note that all terms on the right hand side of the equation can be considered as constant, and that the derivation of the equation assumes that the scanner only contains one radiometer receiver. Since the right hand side of the equation is constant, the uncertainty principle states that measurement precision can be improved at the expense of degrading the spatial resolution of the image. The best precision and finest spatial resolution is achieved by minimizing the right hand side of the equation. This minimizing can be done using several approaches. First, N identical receivers can be introduced into the antenna in order to increase integration time by slowing down the scan rate. This will reduce the right hand side of the equation by the square root of N. Lesser improvement can be achieved by increasing bandwidth, at the risk of being more susceptible to radio frequency interference, and by reducing spacecraft altitude; however, any altitude below 600 km will require re-boosting in order to counteract the effects of atmospheric drag on the lifetime of the orbit. Table 2 presents input parameters and derived parameters for a high precision salinity mapping satellite, with cross track scanning assumed. Note that coarse spatial resolution and multiple feeds are needed to achieve a measurement precision of 0.05 K. In fact, the 4.88 m diameter antenna corresponds to the 16 foot deployable mesh antenna produced by Harris Corp. for the TRDRSS program.

A word of clarification is in order concerning the two separate columns in Table 2. In a cross-track scan mode, the total image swath extends from horizon to horizon. However, the spatial resolution is variable and gradually degrades as the scan angle proceeds from nadir to the horizon. Thus, if we wish to achieve the best spatial resolution for a fixed antenna beamwidth, our data swath must not be too large. If we restrict the scan sector to 50 degrees (± 25 degrees about nadir), the spatial resolution will be no worse than 40 km provided the swath width is restricted to 566 km. On the other hand, if we desire to increase the swath width to have more rapid global coverage, the same data set can be used, at the expense of degrading the spatial resolution. For example, if we open the scan sector to 92 degrees, the swath width is increased to 1315 km, but the resolution worsens to 80

km at the swath edge. If we process data to generate square pixels in the image, we have the capability, at no penalty, to simultaneously produce two data products; a high resolution narrow swath product, or a coarse resolution wide swath product.

The other issue concerns instrument stability. We define stability to mean that the state of the instrument does not change by a specified amount between measurement periods. Thus stability relates to the quality of the instrument calibration procedure and the frequency of the calibration. Our preferred method was presented by Swift and McIntosh [3], as a cartoon which is reproduced here in Figure 2.1. This figure shows a reflector antenna that is spinning about the satellite velocity vector to conduct a cross track scan of the earth beneath. When not viewing the earth, the antenna system views the sky, which is a stable black body radiating at a constant cold temperature of 2.7 K. Instead of a center fed reflector, we would opt for off set scanning geometry in order to eliminate feed blockage and to direct both feed spillover and the main beam into cold space during the calibration period. As a second reference calibration point, we would propose to use an internal warm source, which would be activated during a sector when the antenna is pointed at the sky. Observation of this second reference could be accommodated by switching to a matched

load maintained at a constant and known temperature to within 0.05 K. As an alternative, we prefer to use a stable noise diode to couple a reference signal into the system while simultaneously viewing the cold sky reference. Analysis of the calibration procedure is given later in this section. The SSM/I, which is a well calibrated instrument (which we

Table 2. Design requirements for a high precision salinity mapping satellite.

SPECIFIED PARAMETERS

Max wavelength (m)	0.21	
Antenna diameter (m)	4.88	
Spacecraft altitude (km)	600.00	
Beamwidth constant (deg)	72.00	
Earth radius (km)	6380.00	
Swath scan sector(deg)	50.00	92.00
System bandwidth (MHz)	27.00	
System noise temperature (K)	180.00	

DERIVED PARAMETERS

Satellite velocity (km/s)	7.56	
Antenna beamwidth (deg)	3.10	
Swath width (km)	565.60	1315.08
Resolution at swath edge (km)	40.80	79.98
Spin rate (rpm)		
Double receiver	5.56	
Pixel integration time (ms)		

Double receiver	92.86	23.21
Instrument precision (K)		
Double receiver	0.11	0.06
(Note dTB/dS = 0.5)		

believe comes close to achieving a stability of 0.05 K), is also calibrated at every scan interval by presenting the feed horn with an ambient black body (microwave absorber) and a sub reflector to present cold space. Our worry is that L-Band is such a long wavelength that the loads would encompass a great deal of real estate. As such, the absorber may pose some difficulty in maintaining a constant temperature.

2.1 Receiver Concepts for Increased Precision

In order to accurately measure ocean salinity to an accuracy of 0.1ppt with a microwave radiometer requires a radiometric precision of about 0.05K. Achieving this level of precision is no easy task. First, receiver front-end losses must be minimized in order to provide accuracy to this level. Also important is the stability of the radiometer measurement, which is linked to the type of calibration procedure used. Consistent measurements can only be obtained using a robust calibration technique that is relatively insensitive to changes in device characteristics over time. High stability also requires a

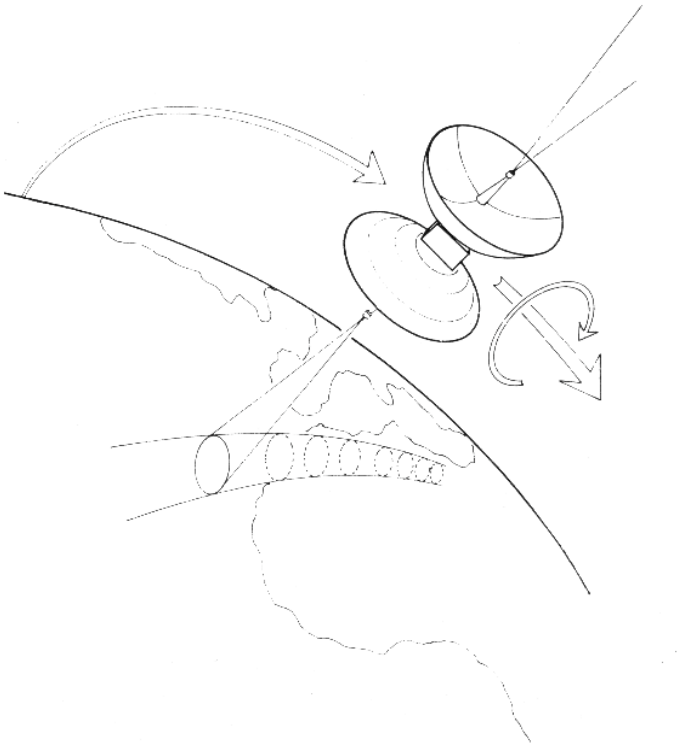

Figure 2.1. Artist's concept of satellite salinity-imaging system.

high degree of temperature control in the radiometer, as temperature fluctuations and gradients can change the characteristics of the calibration standards used.

In this section, we investigate aspects of an L-band radiometer design that affect the stability and precision of the device. These include:

- An evaluation of radiometer precision to determine the required performance of the system components.
- Determination of a practically achievable system noise temperature using commercially available components.
- Discussion of the benefits of an integrated radiometer front-end.
- Investigation of the effect of temperature instability on the radiometric measurement precision.
- Effect of power reflections on the overall noise temperature of the system.
- Introduction of a novel calibration technique which improves radiometric precision and stability.
- A brief discussion of noise diode stability.

2.1 Radiometer Precision

Radiometric precision is degraded by noise contributed from the system components. For passive components, the added thermal noise is proportional to the amount of ohmic loss in the component, according to $T_e=(L-1)T_p$, where L is the power loss factor of the component. For active devices, thermal noise plus noise created by the DC biasing of the device is produced. These sources of noise add to the overall system noise temperature. Other factors, such as system bandwidth and integration time, also affect the precision of the measurement. The precision of the radiometer measurement is given by the equation,

$$\Delta T = \frac{T_A + T_{sys}}{\sqrt{B\tau}} \qquad (1)$$

where T_A is the antenna temperature, T_{sys} is the radiometer system temperature, B is the system bandwidth, and τ is the integration time. At L-band, the radioastronomy quiet band (1.400-1.427GHz) is available, but the system bandwidth is limited to 27 MHz. However, for increased precision, the system bandwidth could be increased to 100 MHz if there is a very low level of RF interference near this band. This is not feasible for measurements over land areas, but should be allowable for sea measurements. The integration time is a function of spin rate, which can not be readily altered to increase precision. However, averaging the measurements obtained for orthogonal polarizations can be used to increase precision. In addition, footprint averaging can be employed to increase precision, but at the expense of decreased measurement resolution. This leaves the radiometer system temperature as the critical parameter to investigate for increased measurement precision.

Using Eq. (3), the required system noise temperature for a measurement precision of 0.05K was computed, and the results are shown in Table 3. An integration time of approximately 93 ms was taken from Table 2. System bandwidths of 27 MHz and 100 MHz were considered, as are the techniques of polarization and footprint averaging. With a 27 MHz bandwidth, the required precision is physically unachievable without averaging. In fact, unless both averaging techniques are employed, the required system noise temperature is below 100K, which is not likely to be achieved in practice. With a 100 MHz bandwidth, noise temperature values that are more realistic are seen, with required system temperatures of above 100 K using either of the averaging techniques.

Strictly speaking, we do not pick up a square root of two improvement in precision due to polarization averaging because the brightness temperature varies with viewing angle as the radiometer system spins about nadir. This variation is due to changes in the Fresnel reflection coefficient with incidence angle, and is therefore predictable.

Table 3. Required receiver noise temperature for a radiometer measurement precision of 0.05 K.

Bandwidth	Eq. (1)	Using Polarization Averaging	Using Footprint Averaging	Using Polarization & Footprint Averaging
27 MHz	-21K	12 K	58 K	124 K
100 MHz	52 K	115 K	205 K	331 K

2.3 Component Summary

Two components that have a large effect on the overall system noise temperature of the standard Dicke radiometer are the low noise amplifier (LNA) and the Dicke switch. The LNA can contribute significant noise to the system, due to the active device. RF switches typically have a high insertion loss, and the main source of noise from the Dicke

switch is thermal noise generated from this loss. Therefore it is critical that the LNA have the best possible noise figure, and the Dicke switch have the minimum insertion loss, to achieve the required radiometer precision.

A survey of commercially available LNA's is shown in Table 4, and a survey of solid-state RF switches is shown in Table 5. Use of monolithic microwave integrated circuit (MMIC) technology allows for excellent performance from both types of components. Insertion loss of less than 1 dB can be obtained from the RF switch, and a noise figure of 0.7 dB (T_{eff} = 51 K) is possible with available LNAs. Using these values, and allowing for small ohmic losses in other receiver components, a total system noise temperature of approximately 115K is obtained. Using the results in Table 3, this value of system temperature can yield the required precision of 0.05K using either a 27 MHz or 100 MHz bandwidth.

2.4 Integrated Radiometer Front-End

Obtaining a low-loss RF switch and an amplifier with a low noise figure are critical to overall system performance. However, other passive system components, such as a bandpass filter and directional couplers, can also increase the system noise temperature. Minimizing reflections and losses in these components will yield the best possible

Table 4. Survey of commercially available microwave switches.

Manufacturer	Switch Type	Insertion Loss (dB)	VSWR	Isolation (dB)	Packaging
MA/COM	SPST Reflective	0.7	1.4:1	40	SMA Female
MA/COM	SPST Absorptive	0.7	1.3:1	50	Surface Mount
MA/COM	Transfer	1.2	1.3:1	35	Surface Mount
Alpha Industries	SPST Absorptive	0.9	1.2:1	40	Surface Mount
MITEQ	Transfer	1.6	1.6:1	55	Surface Mount

Table 5. Survey of commercially available low noise amplifiers.

Manufacturer	Noise Figure (dB)	VSWR	Gain (dB)	Packaging
Delta Microwave	1.1	?	20	SMA Female
Microwave Solutions, Inc.	1.5	?	14	SMA Female
JCA Technology	0.8	2:1	35	SMA Female
MA/COM	1.35	?	26	Surface Mount
MITEQ	0.7	1.3:1	34	SMA Female

performance. Small size of the radiometer front-end is also an attractive characteristic, as it will minimize the thermal gradient, thereby improving thermal stability.

These features can be incorporated in an integrated front-end, as depicted in Figure 2.2. State of the art components available in chip form (switch, LNA, mixer) can be integrated with the other system components in a compact package. If needed, the active devices can be placed on a secondary board to further reduce thermal gradients. High performance microwave substrates can be used to minimize losses. In addition, the passive components and the interconnections to the discrete components can be customized to reduce reflections to a very low level. Another beneficial aspect of the integrated radiometer front-end is that fewer mechanical connectorizations are required. This reduces payload mass and size, and can improve long-term radiometer stability by minimizing the number of transmission line connectors, and again by minimizing thermal gradients.

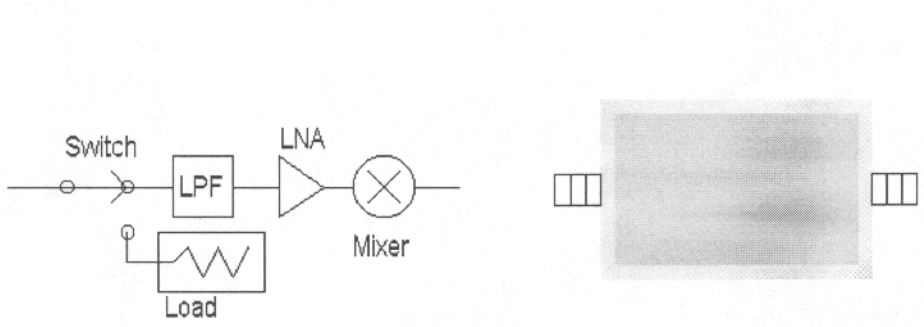

Figure 2.2 Integrated radiometer front-end.

2.5 Radiometer Calibration and Stability

A schematic of the radiometer front-end is shown in Figure 2.3. The Dicke switch and LNA are shown as discrete components, while the other components are modeled as lossy elements. The calibration is carried out by using a cold sky measurement along with a dummy load maintained at a temperature T_o. Losses in the Dicke switch and any

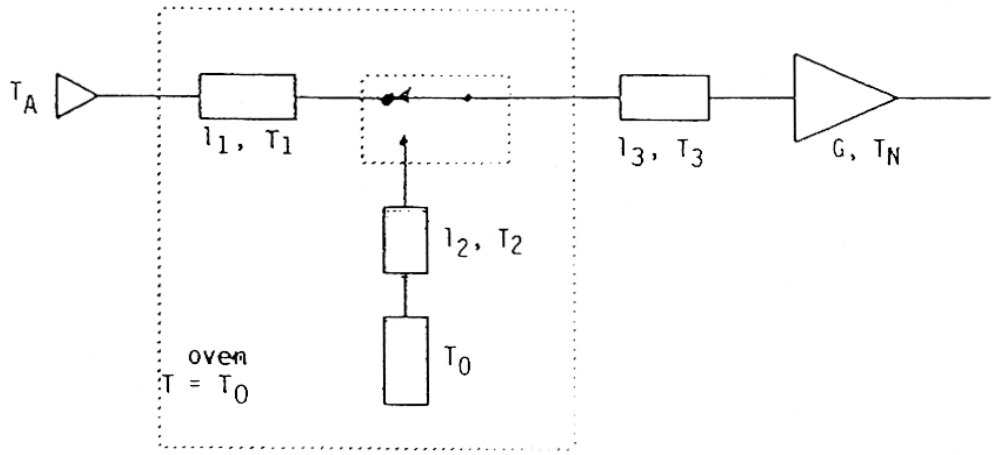

Figure 2.3 Schematic of the radiometer front-end.

components after it are lumped into l_3 and do not affect the stability of the measurement. Losses in the antenna and the interconnects to the switch are lumped into l_1 and l_2. These losses, combined with any temperature gradients that may exist across their associated components, can adversely affect the stability of the radiometer measurement. A plot of the error in the measured brightness temperature versus error in receiver component temperature is shown in Figure 2.4. Errors in receiver component temperature are denoted as ΔT_o , ΔT_1 , or ΔT_2. Also plotted are measurement errors due to linear combinations of these component temperature errors. These linear combinations show the maximum deviation from the desired measurement. This graph shows that a total combined temperature error of less than 0.1K is required for a measurement stability of better than 0.05K.

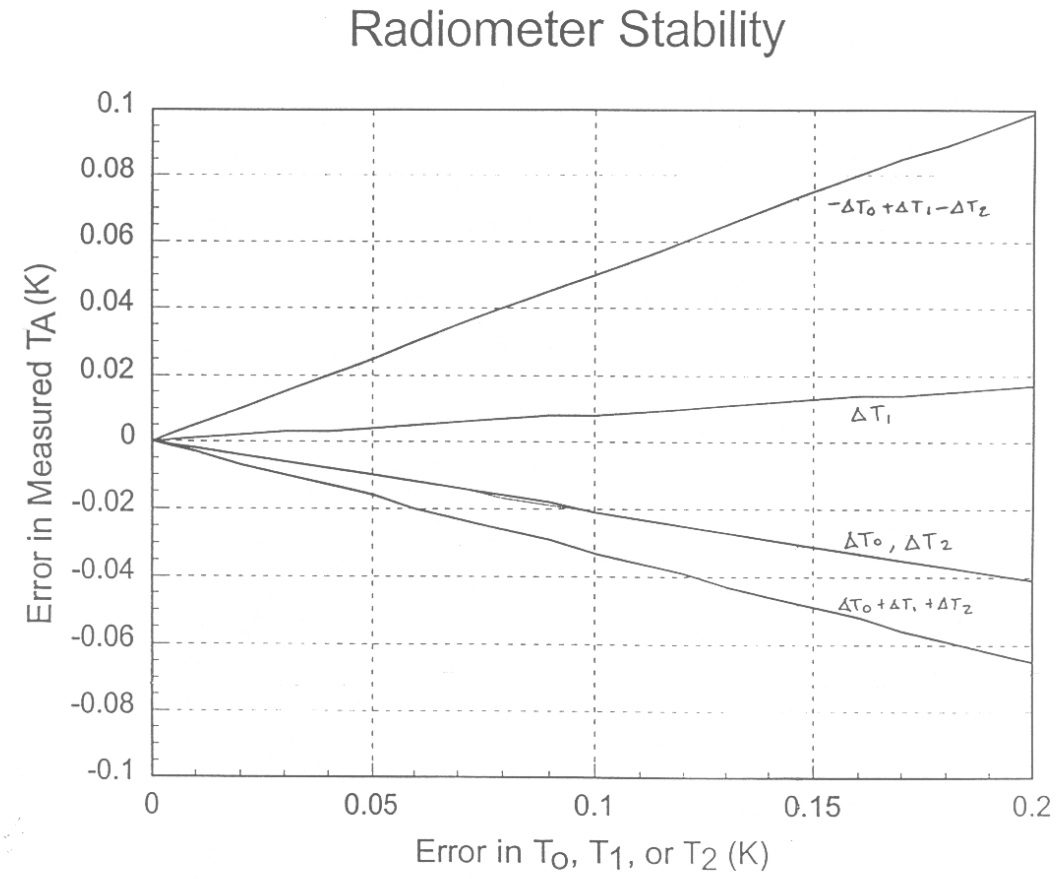

Figure 2.4 Error in measured brightness temperature versus error in T_o , T_1 , or T_2.

Excellent temperature stability of internal components in a radiometer was reported in [4]. The radiometer consisted of two separate chambers; one that contained the RF front-end components, and the second that contained the RF electronics. Each chamber was individually temperature-controlled. The active RF devices (LNA, noise diodes) were insulated from the passive components. Using this configuration, a temperature stability of 0.001K on one-day timescales was reported.

2.6 Effect of Reflections on System Noise Temperature

The effect of reflections on the noise figure of a passive device, for various insertion loss values, is shown in Figure 2.5. The noise figure of a component is related to noise temperature by the relation $F=1+T_e/T_o$, where F is the noise figure, T_e is the effective noise temperature, and in this case a reference temperature of $T_o=T_{ambient}$ is used. Reflections within the system have the property of increasing the system noise temperature and therefore decreasing measurement precision. For the case of L=0.1dB, a

return loss of more than 10 dB causes a negligible increase in noise figure. However, as loss increases the effects of reflections are more apparent. For the case of L=1 dB, a return loss of less than 20 dB causes a significant increase in noise figure. It is seen that by using low-loss components, the effects of reflections within the system are made small. By using a low-loss integrated front-end as depicted in Figure 2.2 with customized impedance matching, the effects of reflections can be made negligible. Adding an isolator at the component input has no beneficial effect on the noise figure; in fact, the insertion loss of the isolator has the potential to significantly increase the noise figure.

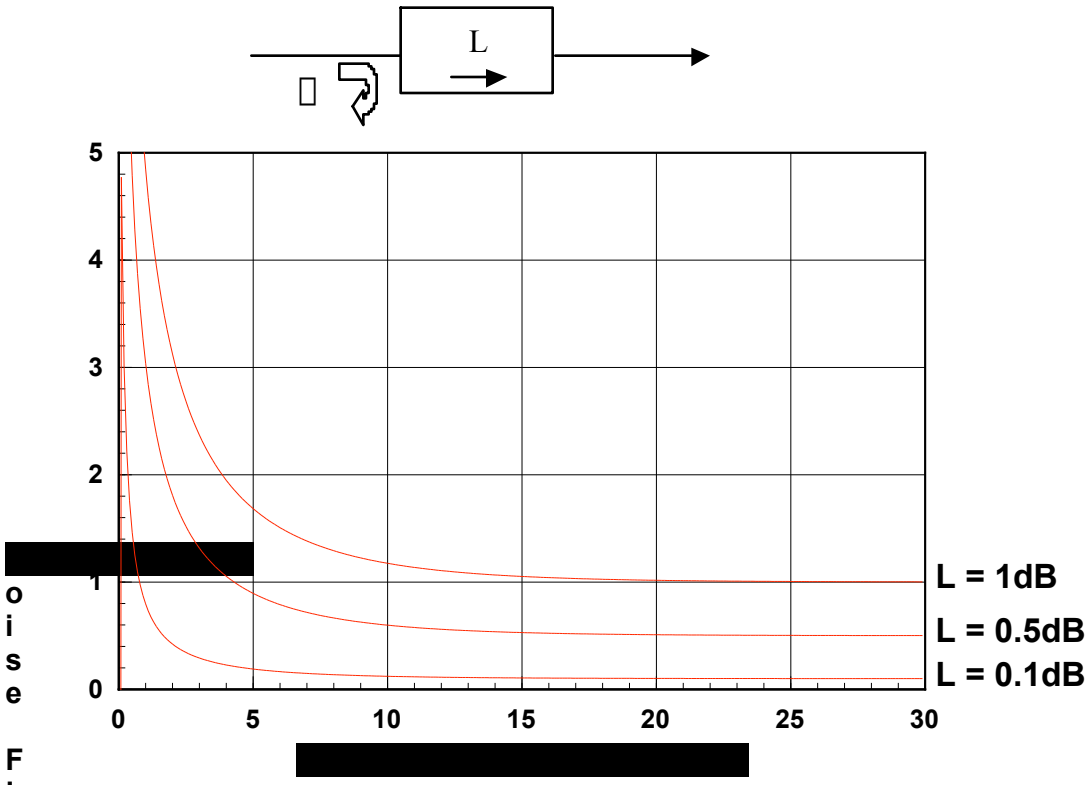

Figure 2.5 Effect of reflections on the noise figure of a passive device, for various insertion loss values. Ambient temperature is 300K

However, the isolator can reduce potential instability in the radiometer measurement by reducing the effect of "backward-travelling" noise [5]. This type of noise can have a varying noise power versus time, or can see an unstable reflection coefficient from a switch or antenna. In either case, these effects cannot be effectively accounted for in the calibration. Sufficient isolation can make the effect of these potential instabilities negligible.

2.7 Alternative System Configuration and Calibration Technique

A schematic of an alternative radiometer front-end, including the calibration equations, is shown in Figure 2.6. This configuration provides an accurate calibration without the need for a Dicke switch, eliminating a large source of loss and potential instability. The calibration is carried out by using a cold sky measurement along with a noise diode having a large excess noise ratio. The power from the noise diode is injected into the system by a directional coupler. The coupling factor is chosen to be close to the ENR of the noise diode, so that the amount of injected noise is approximately equal to that of a dummy load at temperature T_o. An important feature of this design is that it does not require a switch in the main signal path, thus avoiding the loss and associated noise temperature increase of this component.

An interesting characteristic of this configuration and its associated calibration scheme is that noise due to ohmic losses in the antenna itself is always present in the measurement, and can therefore be calibrated out. This is not true of designs utilizing a switch, where only the noise from the antenna or the dummy load can be measured at a given time. This feature eliminates errors due to fluctuations in T_1, if they are slowly varying with time. This is an interesting quality, as it theoretically eliminates instabilities contributed by the antenna emissivity. A plot of the error in the measured brightness versus error in T_3 is shown in Figure 2.7. This plot shows the improved stability of this configuration, as errors due to fluctuations in temperature are effectively reduced by the coupling factor of the directional coupler.

The limiting factor of the configuration of Figure 2.6 is that it is strongly dependent on the stability of the noise diode. A plot of the error in measured brightness temperature versus percentage error in noise diode temperature is shown in Figure 2.8. This shows that there is a linear dependence of the measurement stability on the noise diode stability. For radiometric stability of 0.05K, a noise diode stability of 0.05%, or 500ppm, is required.

The alternative calibration procedure discussed above depends on the stability of the noise diode. According to Tanner [4], several experiments at the Jet Propulsion Laboratory showed noise diode stability on the order of 1000 ppm on one-day timescales. However, further experiments concluded that greater stability could be achieved by using current-regulating bias circuits. Using high-stability current regulation to bias the noise diode yielded a stability of 100 ppm on the same timescales. The noise diode output power is also dependent on temperature, requiring temperature control of the device.
These results are encouraging, since the reported stability of the noise diode is within the required limit for this work.

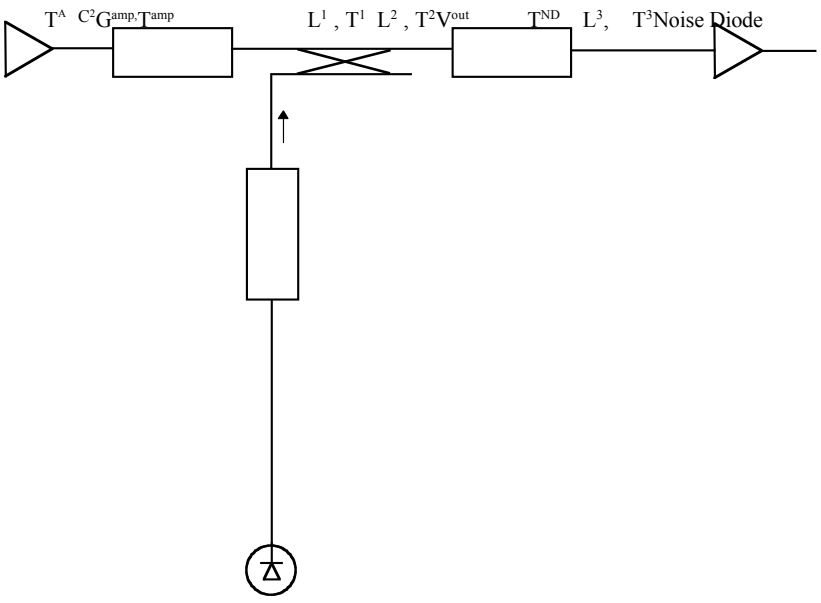

$$V_A = KG_{amp} \{\{[(1-L_1)T_A + L_1T_1] (1-C_2) + C_2L_3T_3\} (1-L_2) + L_2T_2 + T_{amp}\}$$

$$V_N = KG_{amp} \{\{[(1-L_1)T_{sky} + L_1T_1] (1-C_2) + C_2T_{ND}\} (1-L_2) + L_2T_2 + T_{amp}\}$$

$$V_{sky} = KG_{amp} \{\{[(1-L_1)T_{sky} + L_1T_1] (1-C_2) + C_2L_3T_3\} (1-L_2) + L_2T_2 + T_{amp}\}$$

CALIBRATION EQUATION:

$$T_A = T_{sky} + \frac{C_2 (T_{ND} - L_3T_3)}{(1-L_1) (1-C_2)} \frac{V_A - V_{sky}}{V_N - V_{sky}}$$

Figure 2.6 Schematic of an alternative radiometer front-end, including calibration equations.

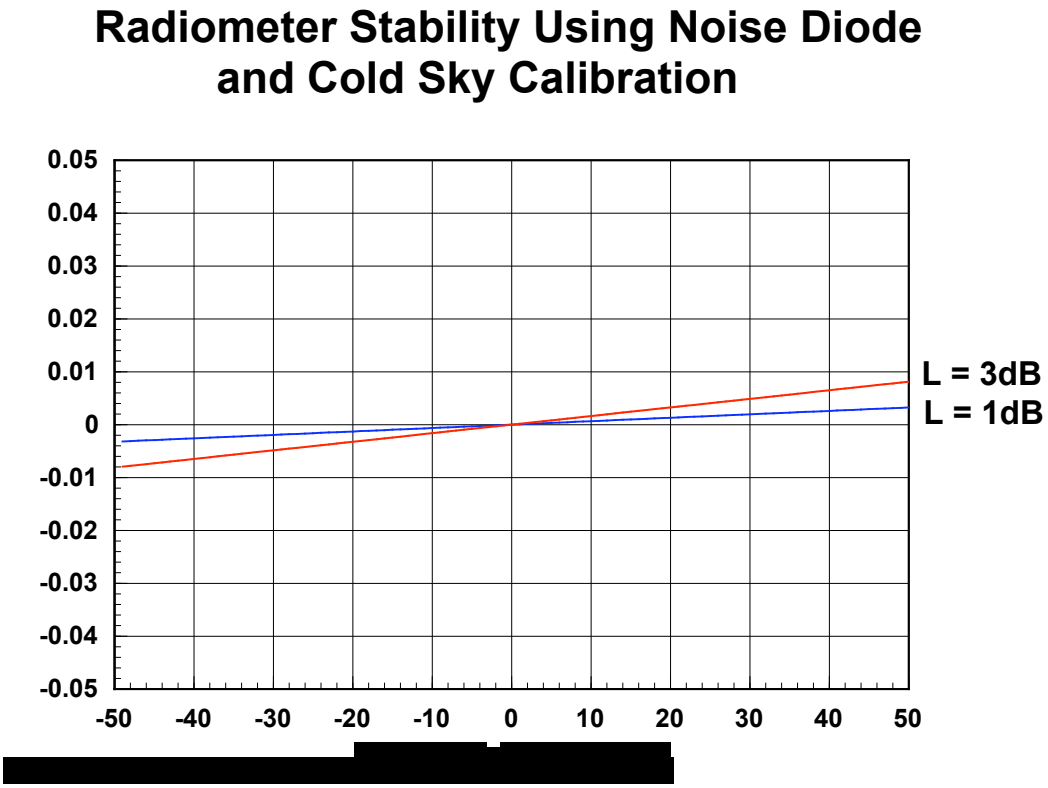

Figure 2.7 Error in measured brightness versus error in T_3.

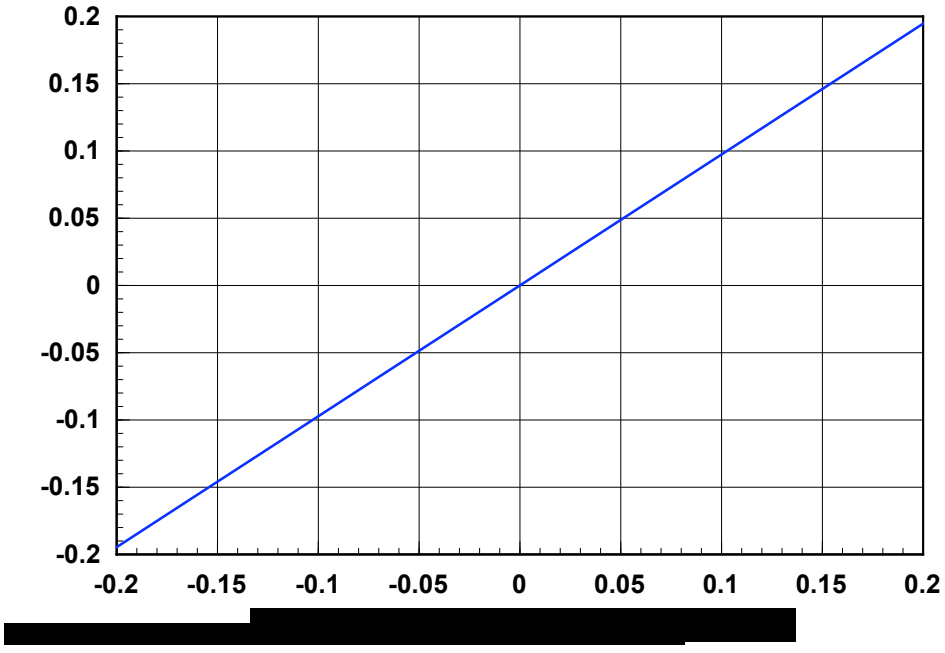

Figure 2.8 Error in measured brightness versus percentage error in noise diode temperature.

2.8 Conceptual Design Summary

The current work has built a foundation from which to achieve high-precision radiometric measurements of ocean salinity. Such measurements require a precision of 0.05 to 0.1K, which in turn requires an extremely low system noise temperature. A main focus of this work is the novel radiometer configuration and calibration scheme that was developed to meet this stringent specification. This configuration is very advantageous for this application in that the Dicke switch is removed from the main signal path. This increases the precision of the radiometer measurement by removing the ohmic losses associated with the switch. Use of this configuration may also eliminate the use of isolators in the design, as the effects of reflections can be calibrated out, theoretically. This will further decrease the system noise temperature and increase precision. Radiometer stability is also increased using this configuration as temperature fluctuations in the main signal path can be calibrated out, and effects of temperature gradients present in the coupled arm to the noise diode are reduced by the directional coupler. Potential instabilities contributed by the switch are also removed from the main signal path.

Further work on this project involves some experimental verification of the theoretical results presented herein. A primary focus is measurement of noise diode stability, as this is critical to the success of the new calibration scheme. Associated with this is an evaluation of temperature control, as this will affect the stability of the noise diode. Other topics to be explored include further study of the integrated front-end and a switchable bandpass filter.

3.0 Considerations for 10 km Spatial Resolution at L-Band

This section reviews the strengths and weaknesses of various measurement methods in spaceborne microwave radiometry leading to the generally acknowledged conclusion that either a pushbroom concept or aperture synthesis offer the greatest potential for achieving high spatial resolution. A review of the conventional wisdom and results from a few trade-off analyses will be used to provide some perspective on this potential.

3.1 Aperture Size

It provides some perspective to begin by considering the relationship between spatial resolution and aperture size for electrically large apertures, given by

$$\text{Spatial Resolution} = \frac{h\,\lambda}{D\cos^2\theta} \qquad (4)$$

where,

h = altitude
β = beamwidth, in radians
θ = incidence angle

This is plotted in Figure 3.1 for a conically scanning real aperture from 600 km altitude. In this case, a 27 m aperture is needed to produce 10 km in spatial resolution. The better point for this study might be that at about 20 m or so (15 km to 20 km in spatial resolution) the curve becomes rather flat and one pays a big price for improvements in spatial resolution.

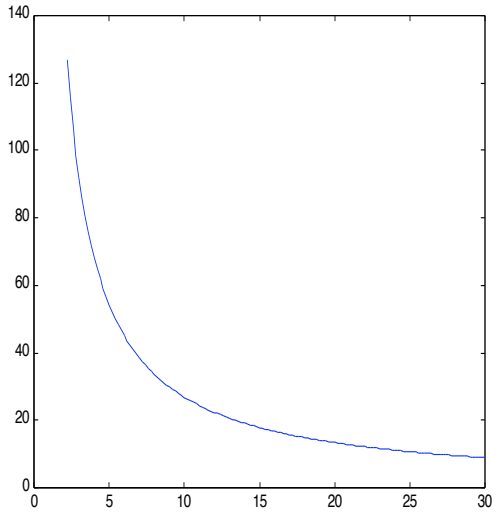

Figure 3.1. Aperture size required at L-Band for 40 degree conical scan.

Typically, spaceborne microwave radiometers have been real aperture systems with mechanically actuated conical scanning to provide the swath and sky calibrations. A typical reflector size has been in the neighborhood of 1 m with scan rates of fractions of a revolution per second. With this type of system, the required scan rate is directly proportional to cross-track spatial resolution and the value of ΔT is directly proportional to scan rate. So, as aperture size increases, both scan rate and ΔT tend to be affected adversely. Multiple beams along track may be used to lower the required scan rate but this too requires an increase in reflector size. In any case, the example shown in Figure 3.1 suggests a 27 m aperture rotating at more than 3 times the SSM/I rate.

3.2 The Conventional Wisdom

Table 6 is useful in reviewing the conventional wisdom for large aperture systems. Disregarding scanning method and concentrating on mass, the 15 m Hoop Column reflector and the 14 m Inflatable Antenna Experiment (IAE) test article can be compared. Both of these were deployable test articles of known mass. Figure 3.2 is an extrapolation of mass vs. aperture size derived from these two systems. It is useful in demonstrating the motivation for developing inflatables and membrane technology for large aperture systems. Below 10 m either technology might provide a reflector less than 100 kg. With all instrument and spacecraft trades considered, the mass difference between the two might not be significant. But for apertures near 30 m the difference is large and the rationale for inflatables is clear.

Table 6. Mass characteristics for various antenna and array technologies.

Antennas and Arrays	Mass Figure	Source Hardware	Study
15 m Hoop Column (Mesh Reflector)	1.4 kg/m^2	✓	
IAE (Inflatable Reflector)	.32 kg/m^2	✓	
36 m Pushbroom			✓
Without Feeds	.19 kg/m^2		
With Feeds	.53 kg/m^2		
1D Synthetic Aperture		✓	
Graphite Epoxy	2.43 kg/m^2		
Tensioned Membrane	.70 kg/m^2		
2D Synthetic Aperture			✓
9 m Aperture	1.11 kg/m^2		
27 m Aperture	.97 kg/m^2		

In 1994, a conceptual design study by Langley and L'Garde, Inc. for a soil moisture mission produced an L-Band pushbroom design with a 36 m inflatable reflector. The mass characteristics were consistent with the IAE and were much better than competing technologies. Additionally, the fundamental thing that is attractive in the pushbroom

concept is that ΔT is not a function of spatial resolution as in scanning and aperture synthesis systems with scan rate and aperture thinning effects, respectively. On the other hand, the 36 m system in this study was so large in order to provide sufficient swath for the required coverage that drag and attitude control problems drove the mission to a higher altitude at the expense of spatial resolution. At least, with this particular design there was an incompatibility meeting both the spatial resolution and coverage requirements.

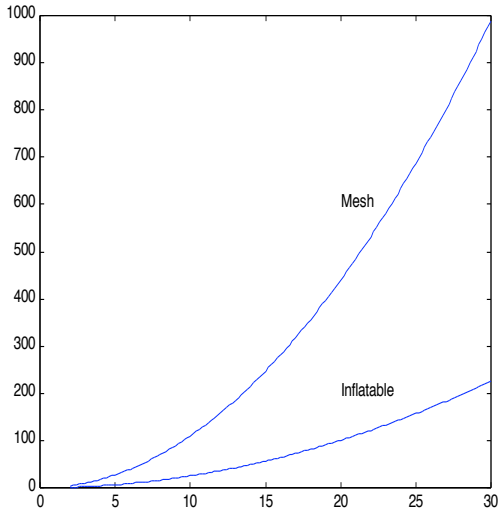

Figure 3.2. Mass comparison for Mesh and Inflatable technologies.

Aperture synthesis, or interferrometric microwave radiometry, is recognized as an alternative technique for high spatial resolution measurements at L-Band. The ESTAR aircraft instrument has demonstrated the capability, a one dimensional system (Hydrostar) has been proposed into the ESSP program, and ESA has sponsored the design of a spaceborne two dimensional system (MIRAS) [6]. The mass per unit area of aperture for a 1D deployable antenna design in composite materials technology is listed in Table 6, along with a much lighter tensioned membrane design pictured in Figure 3.3. The expectation is that the membrane technology offers growth to both polarizations and also offers much smaller packaging for launch. The limitation in currently envisioned tensioned membrane concepts for this application is in the difficulty of growth to multiple frequencies.

Two dimensional systems are expected to offer the advantages of aperture synthesis with both competitive mass characteristics and the potential for growth to 2 or 3 frequencies.

A Langley sponsored conceptual design study for a 9 m, 2D system at L-Band [7] produced the mass characteristics listed in Table 6.

One disadvantage for aperture synthesis, already mentioned, is that ΔT is directly related to array thinning. In principle, ΔT is increased by the ratio of the number of elements in a filled array to the number in the thinned array [8]. The effect on sensitivity is greater for 2D systems than 1D systems due to the greater thinning. Array thinning effects will be discussed quantitatively in a later section. Another disadvantage in aperture synthesis is "fringe washing." This is a decorrelation in the longer baseline measurements that limits bandwidth, swath, and ΔT. For large apertures in the 20 m to 30 m range, fringe washing becomes significant and trade-offs in coverage and ΔT must be made against spatial resolution and instrument complexity.

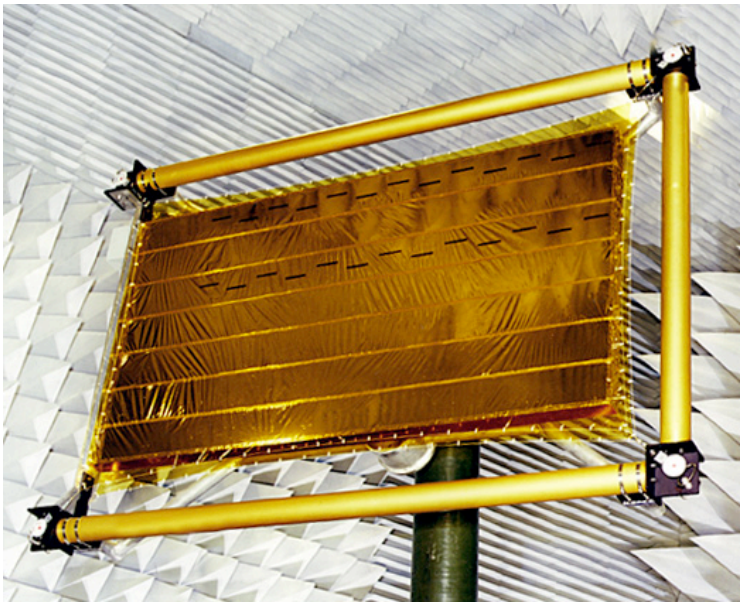

Figure 3.3 Tensioned membrane array feasibility model

In summary, the conventional wisdom is that to achieve 10 km spatial resolution at L-band either the pushbroom technique or aperture synthesis are the logical choices. Therefore, technologies to enable these two measurements with large aperture systems must be developed.

3.3 Mass Estimate for 2D Aperture Synthesis

A detailed mass estimate was included in the 1993 2D, 9 meter L-band conceptual design study, which was for a "cross" configuration, and Figure 3.4 shows the extrapolation of this data as a function of spatial resolution. The spatial resolution shown is resolution at nadir assuming 600 km altitude. The other two points, for a 1D system and the ESA MIRAS system, are included for comparison.

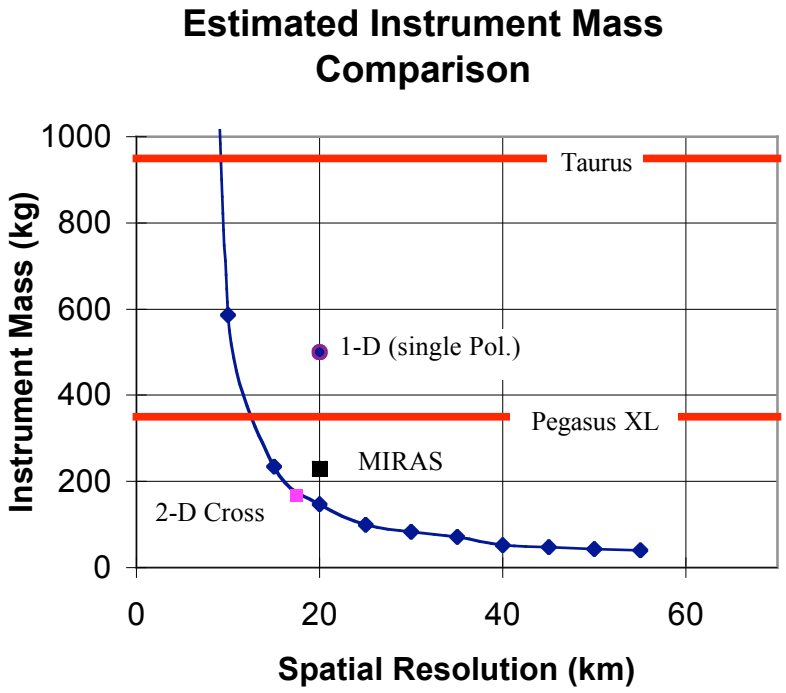

Figure 3.4 Estimated instrument mass

Both of these are estimates from more mature designs than the 2D cross and would be expected to be more accurate. The MIRAS is a "Y" configuration, as well, with fewer receivers than the cross. So, even though the curve is probably an optimistic best case, it makes the point that the mass increase for improvement in spatial resolution to the 10 km range is large, and systems like this wouldn't be candidates for Taurus class $100 M neighborhood missions. The possibilities for achieving up to 15 km resolution in this class mission might be good though.

3.4 Power Requirements with Future Technologies

Current advances in MMIC receiver front-end technology at L-Band lead by the cell phone industry stand to benefit pushbroom and synthetic aperture systems requiring large numbers of receivers. For example, the 2D cross in the 1993 study included 145 receiver channels. Figure 3.5 shows a comparison of an extrapolation of the power requirements from the 1993 2-D L-band conceptual design study with technology

currently being implemented in spaceborne radiometers vs. MMIC technology for future systems. Both of these curves are based on the 2D cross design extrapolated as a function of spatial resolution, and they suggest approximately a factor of 2 reduction in power consumption with the MMIC technology.

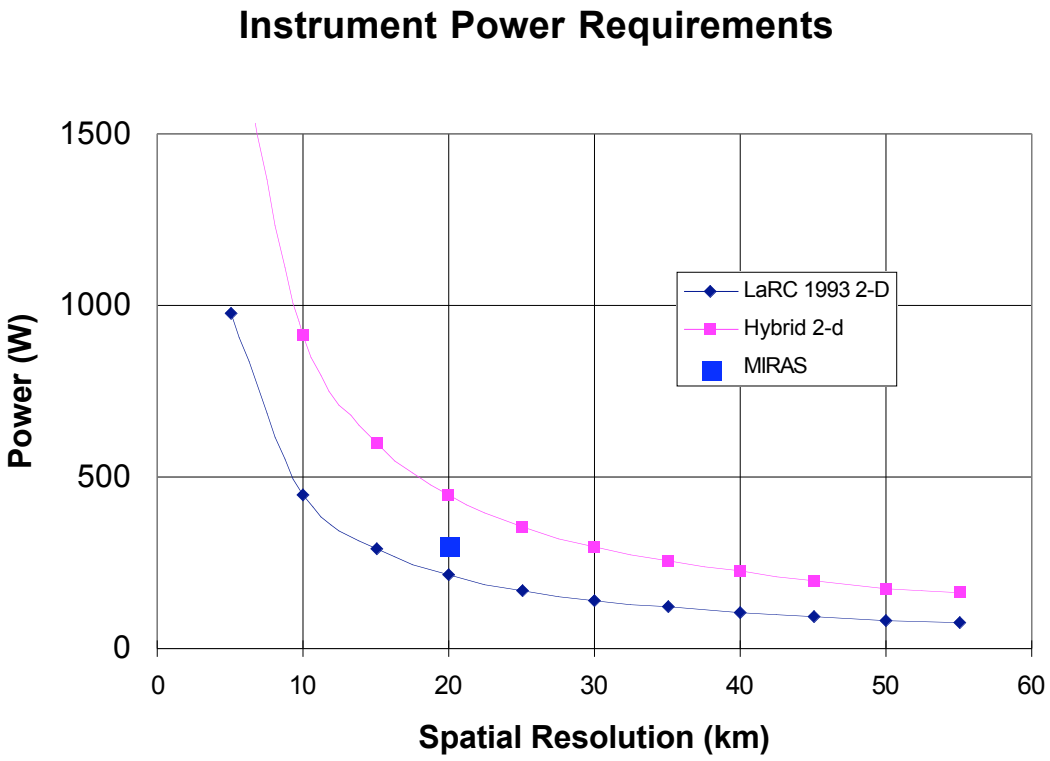

Figure 3.5 Estimated Instrument Power Requirement

3.5 Sensitivity in Aperture Synthesis and Pushbroom

Synthetic aperture systems are thought to suffer a disadvantage in sensitivity compared to scanning total power and pushbroom systems due to array thinning. Actually, the sensitivity of a synthetic aperture system can approach that of a scanning total power system due to the integration time lost by the scanning and the pixel averaging along track in the synthesized image. LeVine [8] compares both 1D and 2D performance to an equivalent real aperture ΔT based on a formulation in terms of a "fill" factor defined as the ratio, A_{sys}/nA_e, where A_{sys} is the effective area of the synthesized antenna, n is the number of elements in the thinned array, and A_e is the effective area of each individual element. LeVine demonstrates, with a particular example, how pixel averaging holds the potential for making 2D performance

comparable to 1D and within a factor of 2 of real aperture performance. This example assumes averaging over the full along-track field of view, which in this case is 200 pixels. Averaging of pixels along-track requires incidence angle and polarization corrections to measurements before averaging and the extent to which the full swath can be used is an issue. MIRAS studies have assumed a 15 degree field of view for averaging. Figure 3.6 shows improvement in ΔT, with averaging, from the case of single pixel measurements along-track (no averaging) to the case of averaging over the full field of view, which is equivalent to the 1D case. The ΔT indicated

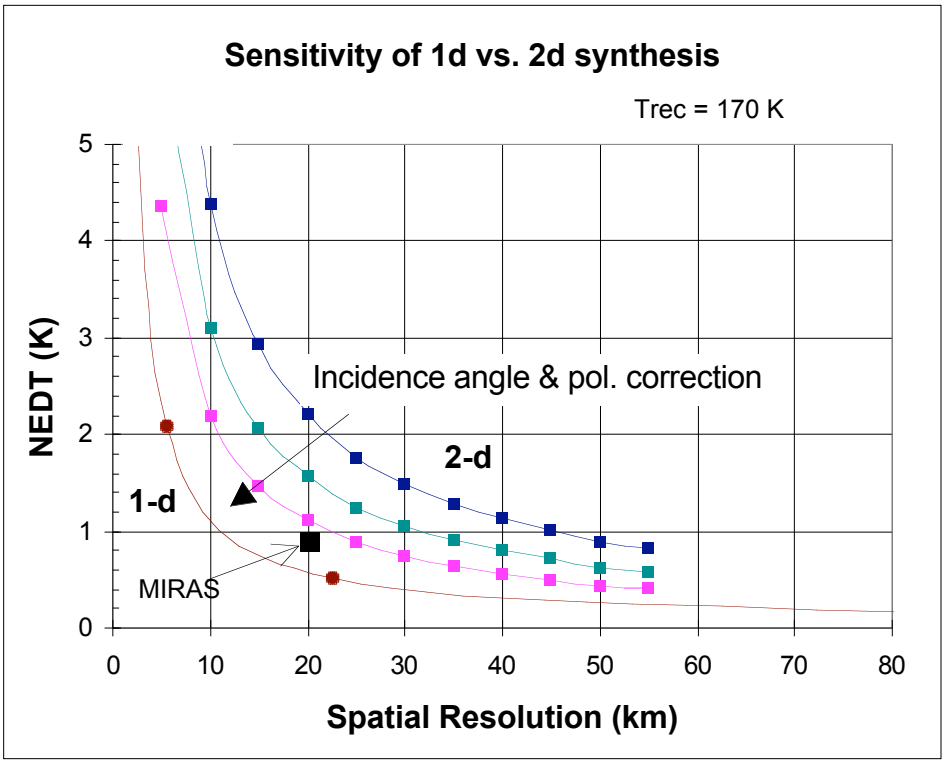

Figure 3.6 Sensitivity in Aperture Synthesis concept.

In Figure 3.6 is for zero redundancy and represents a worst case, since any implementation will include redundant spacings and a 2-D implementation could include λ/2 element spacing along each leg to improve sensitivity. In addition, the size of the individual elements could be increased, reducing the FOV but improving sensitivity. However, this will require increased element spacing and result in "grating lobes" or aliasing due to under sampling the visibility function and must be considered carefully. MIRAS studies [6] have assumed a 15 degree field of view for averaging and have allowed some under sampling. The ΔT reported in [6] is included in figure 3.6 for reference. For reference, the performance of a scanned total power radiometer is equivalent to the 1-D curve

This data suggests that substantial redundancy would be required in a synthetic aperture system to approach the ΔT=0.5 K at 10 km spatial resolution desired for coastal salinity. It is unlikely that a realistic (i.e. sufficiently thinned) 2-D aperture synthesis sensor or a scanned single beam sensor would be sufficient for the coastal salinity mission requirements. A 1-D synthetic aperture system with substantial redundancy or a Pushbroom concept may be the desired approach for this application.

Consider a tensioned membrane array using the technology represented in Figure 3.3, where the deployed array is made up of a blanket of contiguous, uniform, rectangular tubes with dimensions of L-Band waveguide. This system may be configured as either a filled or thinned array for a synthetic aperture measurement. A filled array provides the opportunity to improve the ΔT at the expense of providing a receiver at each element. This tends to defeat the purpose of aperture synthesis. However, with the filled array a pushbroom concept may offer the improved sensitivity with a reduction complexity. Consider time multiplexing the radiometer receivers between image pixels to trade sensitivity for complexity. Figure 3.7 demonstrates the trade between ΔT and complexity for both the 1D aperture synthesis and pushbroom approachs. The bounds for aperture synthesis are given by the "zero redundancy" thinned case and the filled array case with no thinning [9]. For the instrument parameters used to develop this figure, the performance for 1D filled array aperture synthesis is approximately the same as for the pushbroom with N=1. The N=1 case assumes a pushbroom with a receiver for every pixel. Either approach can be configured to improve sensitivity at the expense of complexity. For example, the N=16 case requires an integrated front-end for every array element but time sharing of a single channel by a group of 16 pixels. The number of channels in hardware is determined by the number of array elements divided by 16. The equivalent 1D synthesis approach would require reducing the number of elements in the array by a factor of 4. This will be discussed more fully in Section 5, and it will be demonstrated how new technology developments may make the pushbroom concept preferred, and how a system designed around the tensioned membrane technology could produce the 0.5 K performance at 10 km spatial resolution.

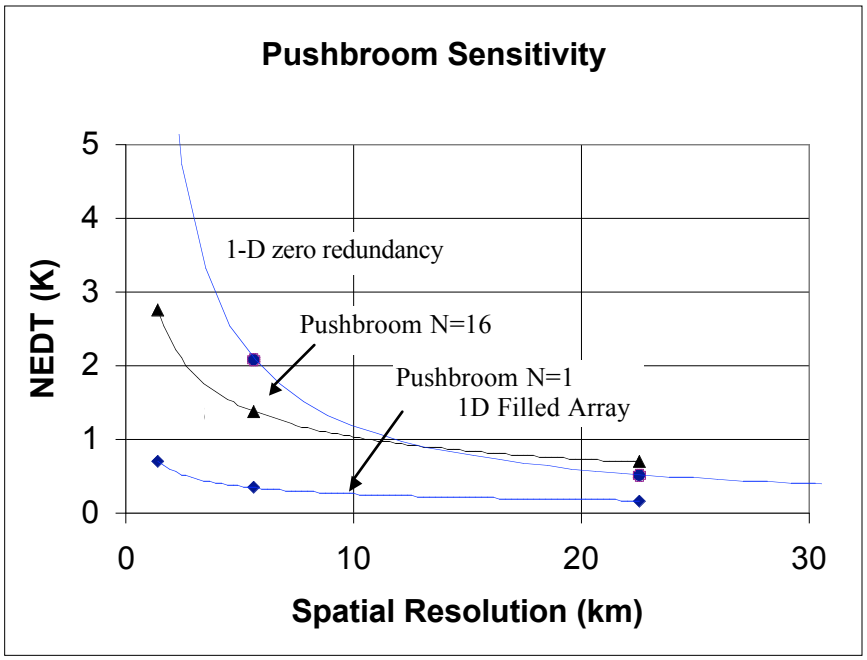

Figure 3.7. Sensitivity of Pushbroom Concept.

3.6 Fringe Washing in Aperture Synthesis

Fringe washing in microwave radiometry is a phenomena that is peculiar to the aperture synthesis interferometer. Fringe washing is a function of the RF bandwidth of the system, which determines the correlation time of the signals [10]. The fringe washing function for a rectangular bandpass characteristic has the form sin x / x where,

$$x = n(\pi/2)\cdot(\Delta f/f_0)\sin\theta \qquad (5)$$

"n" identifies the baseline dimension
$\Delta f/f_0$ = percent bandwidth
θ = incidence angle

One can see that for a sufficiently wide bandwidth decorrelation will occur toward the edges of the swath and in the higher frequency visibility terms. That is, the signal-to-noise ratio will be degraded in the higher frequency terms which will degrade spatial resolution at the swath edges. The effects of fringe washing on the MIRAS design have been analyzed directly in terms of the effect on spatial resolution [11].

It is more appropriate to generalize in this study, so discussion here will just be in terms of the decorrelation factor, sin x / x. Figure 3.8 may be interpreted as decorrelation

at the maximum baseline (highest spatial resolution term) as a function of incidence angle in the cross-track direction. This is for a 2 percent bandwidth, which corresponds to the radio astronomy band at L-Band. From a 600 km orbit a swath of approximately ± 35 degrees is required to meet the revisit time for a soil moisture mission. One can see that in the case shown here significant decorrelation will occur from the outer regions of the swath for apertures in the 20 m to 30 m range. A possible design solution for these large apertures might be bandwidth partitioning in the channels used in the longest baseline measurements. The trade-off is in hardware complexity.

Another trade is between swath width and spatial resolution once some feel for the allowable decorrelation is established. Figure 3.9, for example, suggests potential difficulty in getting 10 km spatial resolution over a swath much more than 15-20 degrees without bandwidth partitioning. The possibility of requiring even more receivers, compounding the electronic complexity of a 2D system, reinforces the need to devise simplified receiver configurations and signal distribution techniques for these instruments.

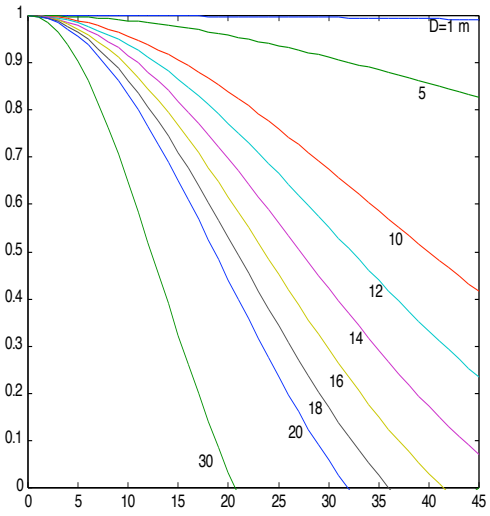

Figure 3.8 Decorrelation at maximum baseline.

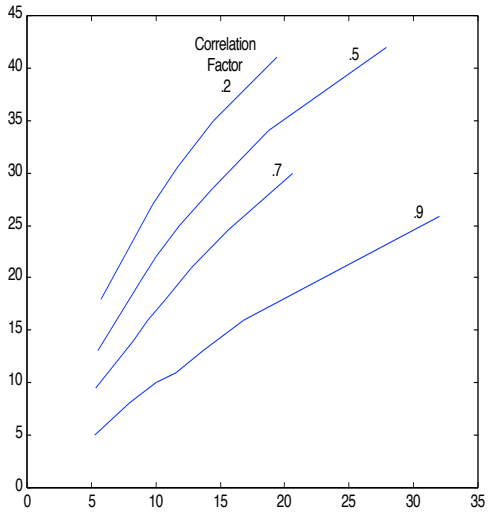

Figure 3.9 Swath and spatial resolution trade.

4.0 Conceptual Design Alternatives in 2D Aperture Synthesis

The aperture synthesis concept has been well known to the radio astronomy community for some time and many complete descriptions of the technique exist in the literature [10]. More recently, aperture synthesis has been applied to earth viewing applications [9]. Aperture synthesis provides the possibility of array thinning (removal of selected elements), while still sampling all spatial harmonics in the scene. This is a major advantage in the synthesis technique, but it also results in degrading ΔT. This degradation of sensitivity due to aperture thinning has been quantified [8,9] and is described in Section 3.5. Many applications of aperture synthesis naturally involve electrically large arrays. Thus, the distribute nature of these systems and the associated phase errors present calibration difficulties. In addition, for 2-D aperture systhesis large number real time of correlations are required.

The objective in this section is to describe instrument design options for use as a basis for discussing instrument performance and identifying instrument technology issues. The results will then be used to identify technology development requirements to specifically address the performance of these instrument concepts. As established in Section 3, the 2D aperture synthesis technique offers the potential for very large aperture, high spatial resolution measurements and it will be the focus for concepts used in this section.

4.1 Arrays and Imaging

As has been discussed aperture thinning appears to degrade instrument sensitivity. However, the 2D technique produces simultaneous pixels over the entire FOV which allows for along-track averaging and in order to determine system level ΔT the additional integration time must be considered. Also, it will be demonstrated in this section how element spacing in a 2D array may be optimized to improve ΔT.

For the purposes of this discussion only, the inherent uncertainty in the estimate of the brightness temperature due to limited integration time is considered. That is, ΔT is the estimate of the mean value of a noise process and calibration, receiver gain, and receiver noise variations are assumed to be small. As discussed above the received voltage from the antenna elements are multiplied together and then averaged to provide a measurement of the complex correlation coefficient of the noise received from the source by each pair of antenna elements. These product terms are noise process with a mean value which are proportional to a spatial frequency component of the scene brightness temperature and a standard deviation which is also a function of the brightness temperature of the entire scene. Determining an analytical expressions for ΔT in the general case is difficult, however, if a uniform brightness temperature scene is assumed then ΔT is given by [9],

$$\Delta T = \left[\frac{(T_o + T_{R1}) \cdot (T_o + T_{R2})}{B\tau} \cdot \frac{(2N_x + 1) \cdot (2N_y + 1)}{2} \right]^{1/2} \quad (6)$$

Where T_{R1} and T_{R2} are the receiver noise temperatures of channel 1 and 2, respectively, B is the predetection bandwidth, τ is the integration time and N_x and N_y are the number of element spacings in the array (1/2 λ spacing). Comparing Equation 6 with the expression for a real aperture total power radiometer, the sensitivity is degraded by the number of independent pixels in the FOV. Equation 6 is for a zero redundancy array and was used for the calculations in Figure 3.6. This data represents a worst case in that zero redundancy arrays are difficult to realize physically and in most cases some redundancy will exist in practical thinned array configurations.

A more complete assessment of the effect of thinning which allows for increasing the size of individual elements (reducing the FOV) and increasing the spacing of the elements yields the result [8].

$$\Delta T = \left[\frac{(T_o + T_{Rec})^2}{2B\tau} \cdot \frac{1}{NM} \sum \frac{A_{syn}}{A_{elem}} \right]^{1/2} \quad (7)$$

where N and M are the number of elements in the x and y directions.

If it is assumed that the element spacing is $\lambda/2$ and that the element pattern is a cosinusoidal function over the real half plane, then the ΔT of a cross configuration, pictured in Figure 4.1,is given buy Equation 6. This insures that grating lobes are in imaginary space, there is no aliasing of the sampled visibility function, and the FOV is limited only by the element pattern. With the assumed 600 km altitude, 170 K receiver noise temperature, and assuming Nyquist sampling, cases assuming no pixel averaging and assuming that every pixel is averaged are included in Figure 3.6. It is, in general, not possible to average all pixels for this configuration since some will not even fall on the earth and many will have such oblique incidence angles that the resulting spatial resolution or incidence angle correction will limit their utility. The use of small individual elements and $\lambda/2$ spacing does not appear optimum for the earth remote sensing case.

A better approach is to reduce the FOV of the individual elements to include the desired swath only, consistent with the element spacing. This provides two advantages. First, the sensitivity is improved as indicated in Equation 7, plus element spacing may be increased reducing the number of receiver channels in the system. Optimizing the element pattern and spacing, plus the use of pixel averaging are improtant in meeting the required sensitivity for an aperture synthesis soil moisture sensor approaching 10 km resolution .

4.2 Instrument Architectures

So far the gain and phase calibration errors in the individual receiver channels have been assumed to be negligible. No instrument effects have been considered. In order to minimize instrument errors, the instrument architecture must be optimized. As shown in Figure 4.1, synthetic aperture systems are highly distributed with portions of every receiver channel located on the array and spread over 10's of square meters in a large aperture system. All of these require interconnections with each other and with centrally located portions of the system, such as power and signal processing. Some of these interconnections carry the received signals and phase reference signals, which are critical in terms of minimizing instrument errors. Consequently, instrument architecture, or configuration, is critical in aperture synthesis.

The configuration in Figure 4.1 is useful for illustration purposes. The module denoted Front-End is physically located at the antenna element and, for example, converts the 27 MHz bandwidth centered at 1413.5 MHz to a digital stream on the order of 120 to 200 Mb/s. This conversion may be accomplished in a number of ways. However, regardless of the specific approach a phase reference signal in the form of a phase coherent LO or a digital sampling trigger will be required at each antenna element. The Front-End will also provide calibration signals which can be injected to measure any changes in the instrument. The Correlator/Accumulator provides the required digital signal processing, communication, and calibration control, which includes the I/Q processing if done digitally.

Assuring gain and phase stability is important since an error in either translates directly to an error in the magnitude and phase of spatial frequency components in the brightness temperature. Analyses in 1D synthesis, for example, indicate that systematic phase errors over the extent of an array, of a fraction of 1 degree for the shortest baselines, would be significant with aperture sizes greater than 10 m. Calibration methods for systems distributed over more than 100 □ are required, and they, along with the error sources themselves, are instrument architecture dependent. In addition to on board calibration, image processing techniques similar to those used in radio astronomy, such as phase closure, the "Clean" algorithm, etc. are of interest. Although these techniques were developed for localized targets, it may be possible to adapt them to extended targets such as those found in earth viewing applications.

There are new device technologies that may particularly benefit these distributed systems, including, for example, low power noise sources, solid state cold sources, and MMIC technology for receiver front-end implementation. The smaller size and mass using MMIC technology provide obvious advantages for space flight application, especially when the number of receivers grows to several hundred. In addition, the reduce size and mass will simplify the thermal control of the front-end which will likely

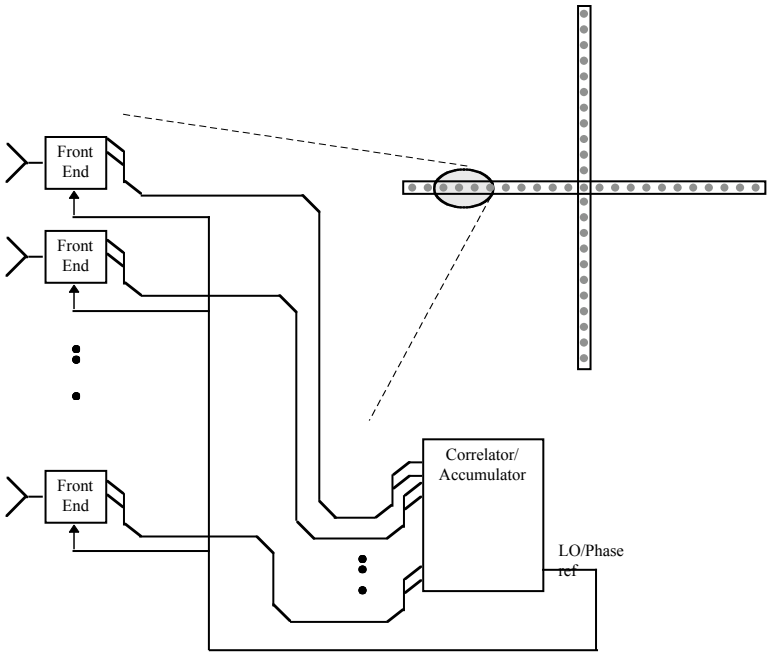

Figure 4.1 Distributed electronics in 2D synthesis

translate in to enhanced stability. Finally, the higher level of integration results in a substantial reduction in power consumption. Again this becomes a major advantage as the number of channels grows. For example, an 8.75 m L-band 2 D synthesis conceptual design study [7] estimated nearly a 100 W (~50%) reduction in required instrument power by utilizing MMIC technology.

Recent advances led by the wireless industry, have reduced the high cost typically associated with this technology for a small number of parts. Although not yet space qualified, low cost MMIC's, which would provide much of the required functionality on a single integrated chip, exist.

4.3 Signal Processing and Correlation

In general there are two ways that the signal processing can be partitioned. The I/Q process can be performed via analog hardware at RF or IF, or the I/Q processing (Hilbert transform) can be performed digitally. These two alternatives are shown in Figure 4.2. In Figure 4.2a, the in-phase and quadrature components (relative to the phase coherent LO) of the input noise process are developed via the analog I/Q down conversion process.

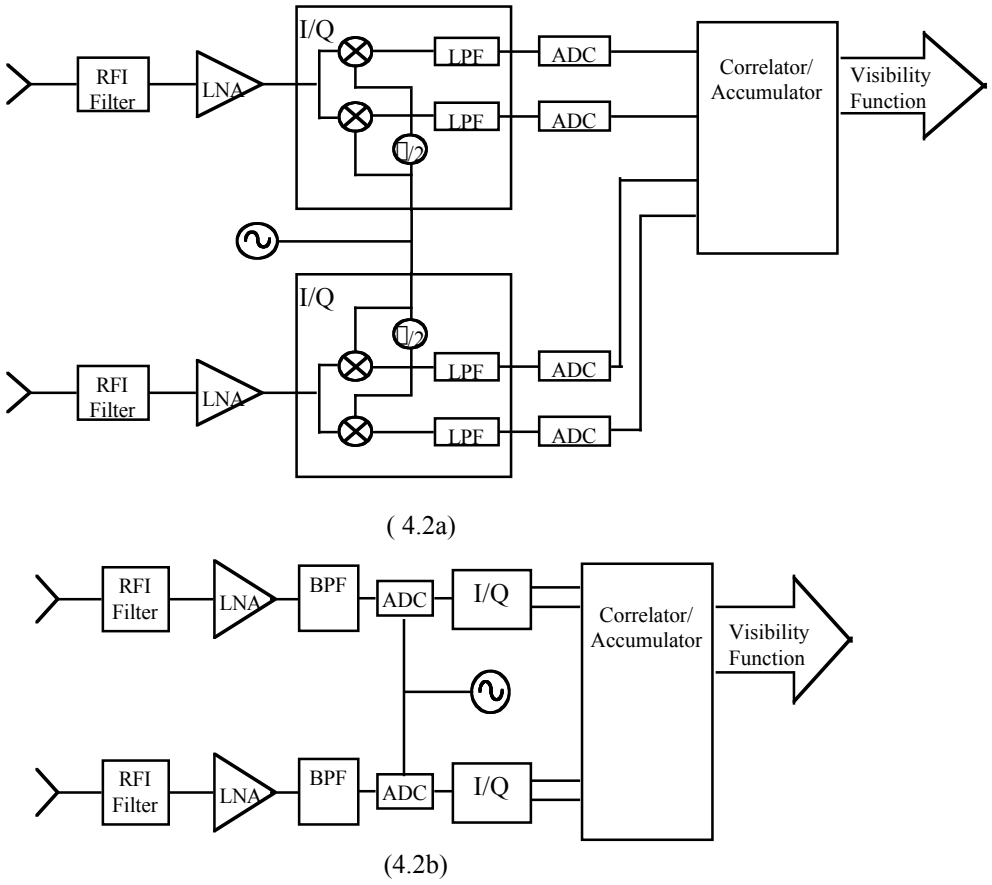

Figure 4.2 Aperture Synthesis Receiver Concepts

These base band In phase and Quadrature signals are then sampled/quantized before being transmitted to the Correlator/ Accumulator.

Figure 4.2b illustrates direct sampling at L-band. Analog to digital converters with sufficient analog bandwidth to sample at 1.4 GHz have been demonstrated [12]. The actual sample rate is selected to meet the narrowband Nyquist criteria and this sampling process effectively provides a down conversion. So the resulting data rate between the Front end and the Correlator/Accumulator is essentially the same as in the analog I/Q approach. Although direct sampling addresses some architecture and interconnect issues, implementing the I/Q process digitally adds significantly to the complexity of the Correlator/Accumulator. Two and three level correlation has also been investigated for digital correlation in aperture synthesis [13], but these studies did not address digital I/Q processing where uncertainties remain.

The digital implementation may substantially reduce I/Q errors and certainly may minimize changes in the amplitude and phase balance of the I/Q process. These errors

relate to assurance that the vectors which are used to describe the in phase and quadrature component have equal length and are orthogonal. Just as with the overall gain and differential phase, the initial error will be absorbed into the "g- matrix," or instrument transfer function, however, any changes which occur once the "g -matrix" is defined will result in an error. The relationship between I/Q errors and estimated brightness temperature must be understood and quantified. Also, directly sampling at L-band and the use of digital processing to provide I/Q requires increased power consumption, which is significant for large apertures. Low power signal processing methods and devices must be developed to enable large systems in aperture synthesis.

5.0 Phased Array Pushbroom

The Pushbroom technique involves the development of multiple beams in the crosstrack direction that simultaneously illuminate a swath of pixels on the surface resembling a pushbroom. Reflector based systems have been analyzed and proposed for space missions, and the Inflatable Antenna Experiment (IAE) demonstrated the deployment of an inflatable reflector. Aircraft phased array pushbroom instruments have been used successfully in field experiments [14]. Historically, for the large arrays of interest here the mass associated with including every element of the array as well as the loss which would occur in the beam forming network all but eliminate this as a candidate approach. However, while these are clearly major challenges, advances in inflatable technologies, such as inflatable reflectors and the inflatable waveguide concept shown in Figure 3.3, as well as, the possibility of low power MMIC LNA /calibration modules have increased the competitiveness of this concept.

5.1 Phased Array Concept

As noted above, the losses associated with the pushbroom beam forming network will typically be unacceptable for radiometer systems. In order to maintain a reasonable system noise temperature an LNA will be required prior to the beamformer. Consider the system configuration shown in Figure 5.1. This system uses waveguide stick elements to provide the along track resolution. The Butler matrix beamformer then combines the received voltages to form the cross track beams. Receivers at the output of the beamformer are essentially total power radiometers. The system concept shown in the figure also includes a calibration module which will provide gain, phase, and receiver noise calibration as discussed below.

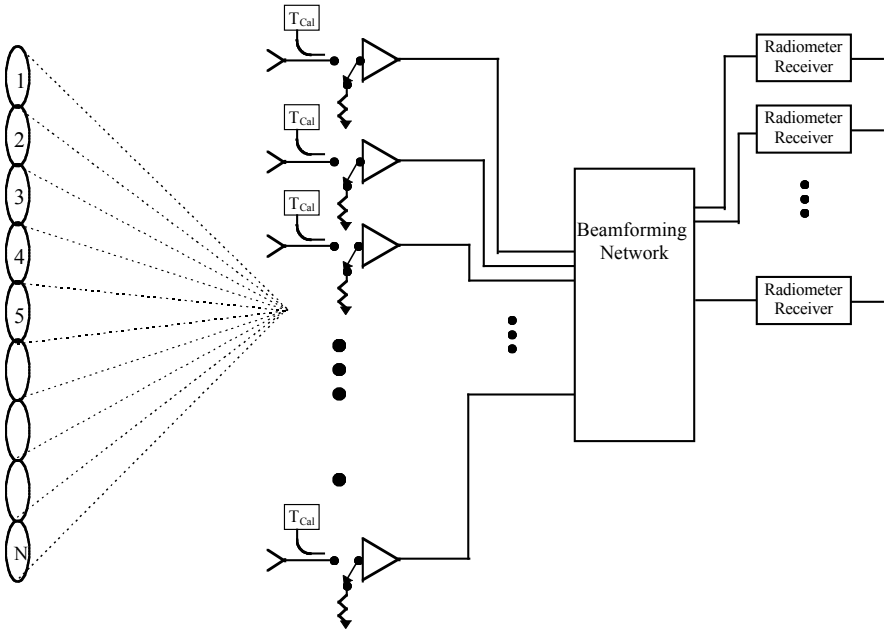

Figure 5.1 Pushbroom Concept

5.2 Stability and Calibration

Again, the phase stability of such an extended system is a concern. When discussed relative to aperture synthesis it is easy to assume phase stability is uniquely an aperture synthesis issue, however, the same concerns exists for the distributed system shown in Figure 5.1. The calibration module must provide a method of correcting for changes in phase. The phase error associated with each element is more difficult to measure and correct than in the case of aperture syntheses since only the output of the butler matrix is measured and beam forming is performed in RF hardware and can not easily be modified.

In addition to the gain and phase correction, the calibration approach must also correct for the receiver noise temperature since total power radiometers are used in the present concept and the receiver noise must be subtracted from the measurement to achieve an estimate of the brightness temperature of the scene. At a conceptual level the receiver noise correction is performed by intermittently switching the input to the LNA's to resistive terminations. The system is then essentially a Dicke radiometer where the difference between the antenna and reference measurements for radiometer channel A could be written,

$$\nu_A^{Ant} - \nu_A^{Ref} = G_A \cdot \left[\sum_{i=1}^{P} g'_i \, T_{Ant} + \sum_{i=1}^{P} g_i T_{Rec_i} - \sum_{i=1}^{P} g_i \left(T_{Ref_i} + T_{Rec_i} \right) \right]$$
$$\nu_A^{Ant} - \nu_A^{Ref} = G_A \cdot \langle g' \rangle \left[T_{Ant} - \frac{\langle g \rangle}{\langle g' \rangle} \langle T_{Ref} \rangle \right] \qquad \textbf{(4.1)}$$

where G_A is the gain of the post beamformer radiometer receiver and $\langle g' \rangle$ is the effective gain of the LNA and beamformer for correlated noise sources at the beamformer inputs. The ratio $\langle g \rangle / \langle g' \rangle$ is the gain reduction factor when the inputs to the system are uncorrelated noise sources. For an ideal butler matrix the ratio should be $P^{-1/2}$ where P is the number of antenna elements. As P becomes large, the sensitivity of the image to errors in the estimate of the ratio or $<T_{ref}>$ increases. This is an issue for the spatial resolution of interest here. The phase and gain calibration problem is very similar to that for the aperture synthesis instrument with the exception that any correction must be provided in hardware prior to the beamformer.

5.3 System ΔT Trades

For a spatial resolution of 10 km (at nadir) the required number of LNA/Cal modules in the phased array pushbroom is approximately 140 and if a radiometer receiver is used for every pixel over a 900 km swath 175 to 180 receivers would be required. As seen in Figure 3.7, the inherent improvement in ΔT provided by the pushbroom concept can be traded for system complexity. Consider time multiplexing radiometer receivers after the beamformer. This would reduce the required number of receivers but degrade the system ΔT by a factor of $N^{1/2}$, where N is the number of multiplexed pixels per receiver. Suppose each receiver is time multiplexed between 8 pixels. Then for a 10 km spatial resolution approximately 22 receivers would be required as shown in Figure 5.2. This selection of N is interesting since it results in the same number of receivers as predicted by the 1-D zero redundancy trend line. The resulting sensitivity shown in Figure 5.3 is approaching the 0.5 K required for coastal salinity.

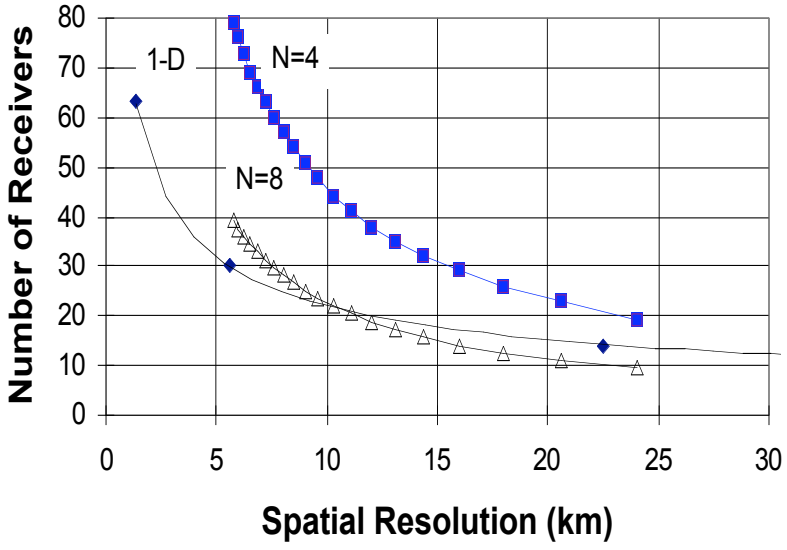

Figure 5.2 Required receivers for 1-D and Pushbroom for selected multiplexing

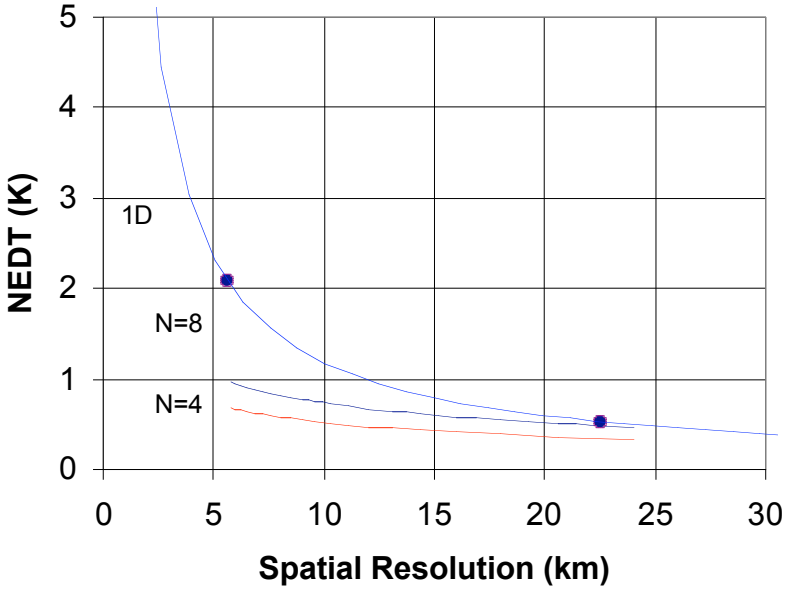

Figure 5.3 Sensitivity for 1-D and Pushbroom for selected multiplexing

The pushbroom approach would required an additional 140 LNA/Cal modules and the aperture synthesis approach would require 9870 complex correlations. Assuming the calibration challenges are equivalent, and low power RFIC technology can be implemented for the LNA/Cal module this concept could provide improved sensitivity which may provide coastal salinity measurement capability and reduce power requirements.

6.0 Technology Development Needs

Previous sections have established a rationale for specific technology development needs for achieving high precision, stability, and spatial resolution in microwave radiometry in the future. For ΔT and stability equal to .05 K and relatively low spatial resolution, scanning real aperture methods have been the focus. For high spatial resolution, 10 km appears difficult to achieve passively for an ESSP class mission. What does seem realistic for ESSP is improving spatial resolution capability to the 15 km to 25 km range, which has been called "adequate" by the users and meets the requirement for many applications in hydrology [1], and the focus here is on 2D synthetic aperture methods. Technology development for this range of spatial resolution would also enable measurements as high as 10 km but with higher complexity and cost. A new pushbroom technique is of interest for providing ΔT=.5 K and spatial resolution in the 20 km to 30 km range.

6.1 Technology Definition Results

Table 7 summarizes the results of this study by listing recommended technology development topics in scanning real aperture, synthetic aperture, and pushbroom systems. These topics are Radiometer Receivers, Array Optimization and Imaging, Instrument Architectures for Distributed Systems, Signal Processing and Correlation, and Deployable Arrays and Materials. Future ESTO technology development should include a microwave radiometry program element, and these 5 topics should make up the content of that program element. Table 7 also lists specific technologies identified in this study as "needed" that serve as examples of proposed projects under each topic. Some of these projects would apply to one of the three measurement techniques, or reference missions, focused on in this study and others would apply to more than just one. Each of the project ideas will be discussed in this section.

Optimization of hybrid configurations and the use MMIC technology in radiometer front-ends is important to all three of the instrument configurations listed here. The pay-off in all cases is in stability, including thermal stability, with additional goals in packaging and lay-out to maximize performance in synthetic aperture and pushbroom arrays and distributed systems. Systems for high precision and stability, that is scanning real aperture and pushbroom, require optimization of measurement methods and front-end configurations for minimizing loss and providing stability in losses, VSWR's, and calibration. The development of low power, highly stable noise sources was identified in Section 2 as critical to achieving .05 K stability, and development of solid state cold sources has potential for providing improved calibration.

Many projects in Table 7 are identified as primarily contributing to synthetic aperture systems, with an emphasis on 2D synthesis for high spatial resolution measurements. Applications at L-band have been emphasized in this study, however technology development at L-band applies to higher frequencies as well. Even though physical size scales inversely with frequency, high spatial resolution implies electrically large apertures so that 10 km spatial resolution at 6.8 GHz for sea surface temperature, for example, is analogous in scale to the L-band examples discussed in Section 3. Optimization of basic array configuration, with respect to such things as element beam shaping, optimization of swath, and array redundancy, is critical in surface sampling to maximize coverage and minimize ΔT. Physically, the variables are such things as array shape, element size, element spacing, and baseline redundancy. In addition, studies are needed in pixel averaging with polarization and incidence angle over the measurement FOV. Analytical studies and simulations over the next 2 years followed by field experiments with the Instrument Incubator Program developed 2D aircraft instrument are needed for array optimization.

With large arrays and distributed systems, such as in aperture synthesis and the phased array pushbroom, total system architecture and configuration become technology issues for instrument stability and calibration. Direct sampling at L-band local to the individual receiver front-ends at each element in the array offers potential for simplifying interfaces and interconnections for large arrays and contributing to phase stability. Maintaining phase calibration is critical for the coherence required in aperture synthesis and the beam forming in a phased array pushbroom. Development and evaluation of candidate analog and digital methods and architectures that minimize complexity and enable phase stability
is required, leading to partial instrument brassboard development in an instrument incubator project.

Digital correlation processing technology is primarily driven by 2D synthesis and would be required for direct sampling at L-band. Low power digital I/Q detection and correlation based on 3 level (2 bits) analog-to-digital conversion is a candidate approach. Devices exist to accomplish thousands of correlations on a single chip. Technology development to meet the I/Q detection requirement and to implement available devices in a digital correlator, leading to an instrument incubator brassboard demonstration project is needed. The development of advanced correlator devices is also needed, although affordability may be an issue for this program.

Lightweight deployable antenna technology with high packing density is needed for both the soil moisture and coastal salinity and the ocean salinity and temperature reference missions. The former requires deployable arrays and the latter requires deployable reflectors. Tensioned membrane deployable array technology is currently being developed by L'Garde, Inc. under an SBIR, and lightweight microstrip technology is being developed under an SBIR at the University of Massachusetts. ESTO technology

development to complement these SBIR's is needed to assure low-losses for earth science applications. Low-loss in reflectors is equally improtant. Therefore, electromagnetic characterization of materials for both arrays and reflector type systems is needed. Characterization of mesh materials is currently planned under a JPL instrument incubator project.

Table 7. Technology Development Needs

Technology Development Needs	Scanning Real Aperture	Synthetic Aperture	Pushbroom
Radiometer Receivers			
MMIC/Integrated Front-Ends	✓	✓	✓
High Precision/High Stability Radiometer Architectures	✓		✓
Low Power/Stable Noise Sources	✓		✓
Array Optimization and Imaging			
Array Configuration/Surface Sampling Optimization		✓	
2D Aircraft Imaging Studies		✓	
Instrument Architectures for Distributed Systems			
Direct Sampling		✓	
Distributed Phase Calibration		✓	✓
Signal Processing and Correlation			
Low Power Digital I/Q		✓	
3 Level Detection and Correlation		✓	
Advanced Correlator Devices		✓	
Deployable Arrays and Materials			
Lightweight Microstrip Arrays	✓		✓
Tensioned Membrane Arrays	✓	✓	
EM Characterization of Materials	✓		✓

6.2 Technology Roadmap

Technology development topics in a) Radiometer Receivers, b) Array Optimization and Imaging, c) Instrument Architectures, d) Signal Processing and Correlation, and e) Deployable Arrays and Materials have been identified as needed for the ESTO technology program. In Figure 6.1, this program is shown having a 1999 start and

including all of these elements. The aperture synthesis path builds on past and current work in the STAR Technology program, the HydroSTAR and MIRAS instrument technologies, and the ESTAR aircraft program. The ESTO technology would quickly feed into an IIP partial brassboard instrument that in parallel with the existing aircraft instrument IIP would position a high resolution soil moisture mission for ESSP. The real aperture/pushbroom path builds on array development in the STAR Technology program and materials characterization being done in a current JPL IIP project, and would run in parallel with 2 related SBIR projects. The ESTO technology would merge with prototype array hardware, from the L'Garde SBIR, and an aircraft salinity mapper, from the U. Mass SBIR, into two IIP projects providing high sensitivity, high stability measurements with improved spatial resolution to ESSP.

This study was fairly broad. Future in-depth studies on 3 measurement concepts that emerged from this effort are recommended. A more detailed design for the real aperture system with the sky calibration scanning mode described in Section 2, for the ocean salinity and sea surface temperature measurement, would complement an existing JPL concept and provide a more solid basis for the technology development. Further study of the two-dimensional aperture synthesis method is needed to determine the maximum realistic expectation for spatial resolution in an ESSP soil moisture mission, adding sufficient detail in design and performance to really focus the technology development. A more thorough study of the phased array pushbroom concept is needed to adequately assess its potential for making a coastal salinity measurement.

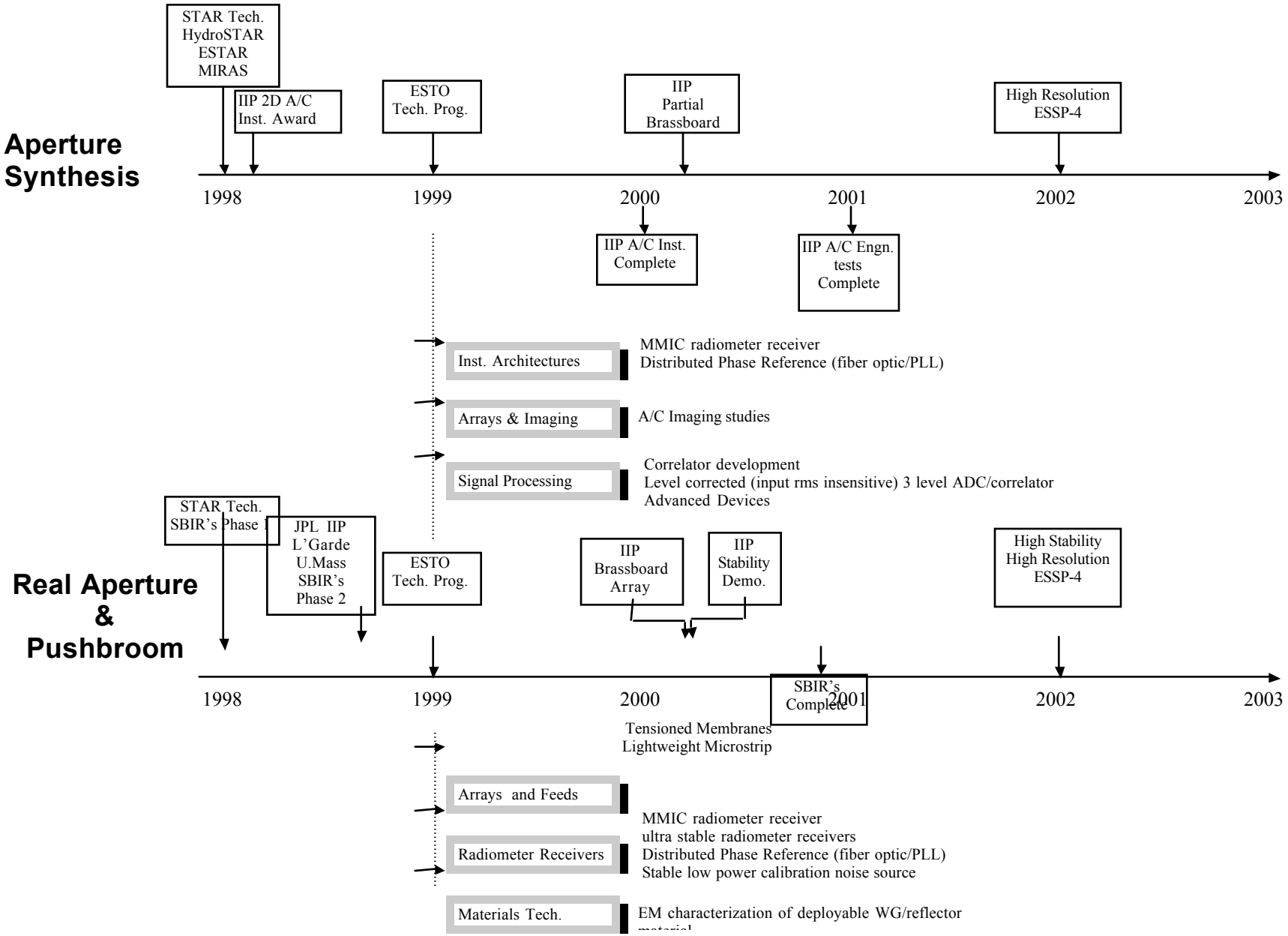

Figure 6.1 Technology Road Map

References

[1] High-Resolution Multifrequency Microwave Radiometer, Earth Observing Sustem Volume IIe, Instrument Panel Report, NASA, 1987.

[2] F.T. Ulaby, R.K. Moore, and A.K. Fung, Microwave Remote Sensing: Active and Passive, Vol. 1., pp. 424-427, Addison Wesley, 1981.

[3] C.T. Swift and R.E. McIntosh, "Considerations for Microwave Remote Sensing of Ocean-Surface Salinity", IEEE Transactions on Geoscience and Remote Sensing, Vol. GE-21, No. 4, pp. 480-491, October 1983.

[4] A.B. Tanner, "Development of a high-stability water vapor radiometer", *Radio Science*, Vol. 33, No. 2, pp 449-462, Mar.-Apr. 1998.

[5] W.N. Hardy, K.W. Gray, and A.W. Love, "An S-Band radiometer design with high absolute precision", *IEEE Transactions on Microwave Theory and Techniques*, Vol. MTT-22, No. 4, pp. 382-390, April 1974.

[6] M. Martin-Neira and J.M. Goutoule, "MIRAS - A two- dimensional aperture synthesis radiometer for soil moisture and ocean salinity observations", ESA Bulletin 92, pp. 95-104, November 1997.

[7] P. Mutton et.al, "A conceptual design study for a two-dimensional, electronically scanned thinned array radiometer", *NASA TM 109051*, November 1993.

[8] D.M. LeVine, "The sensitivity of synthetic aperture radiometers for remote sensing applications from space", *Radio Science*, Vol. 25, No. 4, pp. 441-453, July-August 1990.

[9] C.S. Ruf, C.T Swift, A.B. Tanner, and D.M. LeVine, "Interferometric synthetic aperture microwave radiometry for the remote sensing of the earth", *IEEE Trans. Geosci. Remote Sensing,* Vol. 26, No. 5, pp. 597-611, September 1988.

[10] A.R. Thompson, J.M. Moran, and G.W. Swenson, Jr., *Interferometry and Synthesis in Radio Astronomy*, John Wiley, New York, 1986.

[11] J. Bara, A. Camps, F. Torres, and I. Corbella, "Angular resolution of two dimensional, hexagonally sampled interferometric radiometers,"*Radio Science*, Vol. 33, No. 5, pp. 1459-1473, September-October 1998.

[12] M.A. Fischman and A.W. England, "A direct-sampling receiver for synthetic thinned array radiometry," Proc. Ieee IGARSS '98, Vol. III, pp. 1711-1713, July 1998.

[13] C.S. Ruf, "Digital correlators for synthetic aperture interferometric radiometry," *IEEE Trans.Geosci. Remote Sensing, Vol.33, NO.5, pp. 1222-1229, September 1995.*

[14] R.W. Lawrence, et al., "Design and development of a multibeam 1.4 GHz pushbroom microwave radiometer," NASA TM 89005, September 1986.